EFFICIENT EXTRACTION AND EVALUATION OF COMPLEX PAVEMENT MARKINGS FROM MOBILE LASER SCAN DATA

FINAL PROJECT REPORT

by

Jaehoon Jung, Research Associate
Michael J. Olsen, PI
Erzhuo Che, Post-Doctoral Scholar
Christopher Parrish, Co-PI
Oregon State University

Sponsorship
Pacific Northwest Transportation Consortium (PacTrans)

for

Pacific Northwest Transportation Consortium (PacTrans)
USDOT University Transportation Center for Federal Region 10
University of Washington
More Hall 112, Box 352700
Seattle, WA 98195-2700

In cooperation with U.S. Department of Transportation,
Office of the Assistant Secretary for Research and Technology (OST-R)

DISCLAIMER

The contents of this report reflect the views of the authors, who are responsible for the facts and the accuracy of the information presented herein. This document is disseminated under the sponsorship of the U.S. Department of Transportation's University Transportation Centers Program, in the interest of information exchange. The Pacific Northwest Transportation Consortium, the U.S. Government and matching sponsor assume no liability for the contents or use thereof.

TECHNICAL REPORT DOCUMENTATION PAGE

1. Report No.	2. Government Accession No.	3. Recipient's Catalog No.
	01701479	

4. Title and Subtitle	5. Report Date
Efficient Extraction and Evaluation of Complex Pavement Markings from Mobile Laser Scan Data	June 15, 2020
	6. Performing Organization Code

7. Author(s) and Affiliations	8. Performing Organization Report No.
Jaehoon Jung, Ph.D., Oregon State University Michael J. Olsen, Ph.D., Oregon State University; 0000-0002-2989-5309 Erzhuo Che, Ph.D., Oregon State University Christopher Parrish, Ph.D., Oregon State University; 0000-0002-2681-0090	2018-S-OSU-3

9. Performing Organization Name and Address	10. Work Unit No. (TRAIS)
PacTrans Pacific Northwest Transportation Consortium University Transportation Center for Federal Region 10 University of Washington More Hall 112 Seattle, WA 98195-2700	**11. Contract or Grant No.** 69A3551747110

12. Sponsoring Organization Name and Address	13. Type of Report and Period Covered
United States Department of Transportation Research and Innovative Technology Administration 1200 New Jersey Avenue, SE Washington, DC 20590	Final Report (08/16/2018 to 08/15/2020)
	14. Sponsoring Agency Code

15. Supplementary Notes

Report uploaded to: www.pactrans.org

16. Abstract

Pavement markings are an important traffic control device, enhancing both the safety and efficiency of various modes of transportation by aiding vehicles, bicyclists, and pedestrians in effectively navigating the transportation network. In this PacTrans project, we developed a new framework to extract and classify various road markings from mobile laser scanning (MLS) data. The proposed framework consists of three principal steps: road surface extraction, road marking extraction, and road marking classification. For road surface extraction, using geometric information from the point cloud, ground filtering followed by slope filtering are applied to extract a road surface that is likely to include road markings. Next, the extracted road surface point cloud data are rasterized with Otsu's method into 2D to generate an intensity image and segment high-intensity pixels, likely representing road markings. To reduce false positives while preserving the actual road markings, we apply the block partition and high-pass filtering approaches. Finally, for road marking classification, common linear lane markings with lengths greater than a predefined threshold are first segmented, and then remaining markings are fed into a template matching program for classification. The developed program was evaluated by using a variety of MLS data collected by the Oregon Department of Transportation (ODOT). The experimental results showed that the developed program outperformed our previous version of the road marking extraction tool by extracting highly curved and complex road markings with significantly fewer false positives. The developed program can be used to support informed decision making by state transportation agencies for effective management of road markings.

17. Key Words	18. Distribution Statement
Laser radar, Road markings, Segmentation, Classification	

19. Security Classification (of this report)	20. Security Classification (of this page)	21. No. of Pages	22. Price
Unclassified.	Unclassified.	32	N/A

Form DOT F 1700.7 (8-72) **Reproduction of completed page authorized.**

SI* (MODERN METRIC) CONVERSION FACTORS

APPROXIMATE CONVERSIONS TO SI UNITS

Symbol	When You Know	Multiply By	To Find	Symbol
		LENGTH		
in	inches	25.4	millimeters	mm
ft	feet	0.305	meters	m
yd	yards	0.914	meters	m
mi	miles	1.61	kilometers	km
		AREA		
in^2	square inches	645.2	square millimeters	mm^2
ft^2	square feet	0.093	square meters	m^2
yd^2	square yard	0.836	square meters	m^2
ac	acres	0.405	hectares	ha
mi^2	square miles	2.59	square kilometers	km^2
		VOLUME		
fl oz	fluid ounces	29.57	milliliters	mL
gal	gallons	3.785	liters	L
ft^3	cubic feet	0.028	cubic meters	m^3
yd^3	cubic yards	0.765	cubic meters	m^3
	NOTE: volumes greater than 1000 L shall be shown in m^3			
		MASS		
oz	ounces	28.35	grams	g
lb	pounds	0.454	kilograms	kg
T	short tons (2000 lb)	0.907	megagrams (or "metric ton")	Mg (or "t")
		TEMPERATURE (exact degrees)		
°F	Fahrenheit	5 (F-32)/9 or (F-32)/1.8	Celsius	°C
		ILLUMINATION		
fc	foot-candles	10.76	lux	lx
fl	foot-Lamberts	3.426	$candela/m^2$	cd/m^2
		FORCE and PRESSURE or STRESS		
lbf	poundforce	4.45	newtons	N
lbf/in^2	poundforce per square inch	6.89	kilopascals	kPa

APPROXIMATE CONVERSIONS FROM SI UNITS

Symbol	When You Know	Multiply By	To Find	Symbol
		LENGTH		
mm	millimeters	0.039	inches	in
m	meters	3.28	feet	ft
m	meters	1.09	yards	yd
km	kilometers	0.621	miles	mi
		AREA		
mm^2	square millimeters	0.0016	square inches	in^2
m^2	square meters	10.764	square feet	ft^2
m^2	square meters	1.195	square yards	yd^2
ha	hectares	2.47	acres	ac
km^2	square kilometers	0.386	square miles	mi^2
		VOLUME		
mL	milliliters	0.034	fluid ounces	fl oz
L	liters	0.264	gallons	gal
m^3	cubic meters	35.314	cubic feet	ft^3
m^3	cubic meters	1.307	cubic yards	yd^3
		MASS		
g	grams	0.035	ounces	oz
kg	kilograms	2.202	pounds	lb
Mg (or "t")	megagrams (or "metric ton")	1.103	short tons (2000 lb)	T
		TEMPERATURE (exact degrees)		
°C	Celsius	1.8C+32	Fahrenheit	°F
		ILLUMINATION		
lx	lux	0.0929	foot-candles	fc
cd/m^2	$candela/m^2$	0.2919	foot-Lamberts	fl
		FORCE and PRESSURE or STRESS		
N	newtons	0.225	poundforce	lbf
kPa	kilopascals	0.145	poundforce per square inch	lbf/in^2

*SI is the symbol for the International System of Units. Appropriate rounding should be made to comply with Section 4 of ASTM E380.
(Revised March 2003)

TABLE OF CONTENTS

LIST OF FIGURES

LIST OF TABLES

LIST OF ABBREVIATIONS

GNSS:	Global Navigation Satellite System
ML:	Mobile lidar
MLS:	Mobile laser scanning
MTLS:	Mobile terrestrial laser scanning
ODOT:	Oregon Department of Transportation
PacTrans:	Pacific Northwest Transportation Consortium
ROME:	Road marking extraction
WSDOT:	Washington State Department of Transportation

ACKNOWLEDGMENTS

The authors thank Daniel Wright, Rhonda Dodge, and Lloyd Bledsoe from Oregon DOT for providing the mobile lidar data sets used in this study. Jon Lazarus and Jennifer Lanzarotta also provided helpful ideas and feedback. Oregon DOT also provided funding (SPR-799) for the development of ROME 1.3, which provided the foundation for this research. The authors also thank Leica Geosystems, Maptek I-Site, and the developers of CloudCompare for providing software utilized in this study.

EXECUTIVE SUMMARY

Pavement markings are an important traffic control device, enhancing both the safety and efficiency of various modes of transportation by aiding vehicles, bicyclists, and pedestrians in effectively navigating transportation networks. The importance of pavement markings continues to grow, as autonomous vehicles, which show great promise to improve mobility in transportation networks, utilize pavement markings detected through video feeds to help appropriately position themselves in the lane. Some pavement markings are required to be made of retroreflective materials to ensure their nighttime visibility, but they degrade because of vehicles passing over them and weathering. Transportation agencies must periodically assess the condition of these markings to ensure that they meet specifications. These evaluations are typically performed by using a handheld or mobile retroreflectometer, or through visual, qualitative assessment. Each of these existing methods has associated limitations, related to various factors such as safety, cost, time, and repeatability.

A potential alternative is the use of mobile laser scanning (MLS) data. Many transportation agencies currently conduct surveys of roadways with MLS on a regular basis, and lidar intensity (return signal strength) data can be used to estimate the retroreflectivity of pavement markings in support of condition evaluations. In a recent project with the Oregon Department of Transportation (ODOT), the research team developed an automated method to extract linear lane markings from MLS data and to evaluate the retroreflectivity of those markings. In this PacTrans project, we built upon that effort to develop advanced techniques to handle more complex markings (e.g., pedestrian crosswalk markings, bicycle markings, and arrows) that were not considered in the previous ODOT project but nevertheless are still important for supporting mobility for multi-modal transportation.

Broadly, the proposed approach can be divided into three principal steps: road surface extraction, road marking extraction, and road marking classification. For road surface extraction, on the basis of the rich geometric information from a point cloud, ground filtering followed by slope filtering are applied to extract the road surface data that are likely to include road markings. Next, by using the radiometric information available (i.e., point cloud intensity), the extracted road surface point cloud data are rasterized into 2D to generate an intensity image. Otsu's segmentation is subsequently used on this image to segment high-intensity pixels, likely representing road markings. Because the intensity values are sensitive to changes in the range and incidence angles, the segmentation initially includes some incorrect markings. To reduce those incorrect markings while preserving actual road markings, high-pass filtering and an iterative morphological bridge operation are applied. Finally, in road marking classification, common linear lane markings with lengths greater than a predefined threshold length are first segmented, and the remaining markings are then classified by using a template matching model. To generate training data for the matching process, we collected a set of templates from MLS data and also created additional synthetically modified data by using a data augmentation approach to account for a variety of marking conditions, such as different orientation, skewness, and scale.

The developed algorithm was evaluated by using a variety of MLS data collected by ODOT's current mobile lidar system, a Leica Pegasus:Two. Experiments demonstrated that the developed program outperformed our previous version of the road marking extraction tool (RoME v1.3- developed in previous research for ODOT) in speed, accuracy, and the types of markings that can be extracted. The new algorithm was shown to be capable of extracting highly

curved and complex road markings while still significantly reducing false positive and false negative markings.

By providing detailed information, including spatial coordinates and types of markings, the extracted road marking data will enable transportation agencies to use performance-based procedures to evaluate pavement marking quality. This, in turn, will support informed decision making by DOT management for effective resource allocation. Improved maintenance of pavement markings will also lead to improved mobility with technologies such as autonomous vehicles.

CHAPTER 1. Introduction

Mobile lidar (ML, also called mobile laser scanning, MLS, or mobile terrestrial laser scanning, MTLS), hereafter referred to as MLS, systems can acquire detailed 3D data efficiently from a moving vehicle at highway speeds with traffic. Figure 1.1 shows an example of a mobile lidar system (Leica Pegasus:Two), which is currently operated by the Oregon Department of Transportation (ODOT). Lidar provides several benefits and, as a result, is being widely adopted by departments of transportation across the country (Olsen et al. 2013a&b, 2018). One of the key benefits of lidar is the fact that the same lidar data set can be used by multiple people for a wide variety of applications, minimizing the need for multiple data collections. This versatility has resulted in the phrase, "collect once, use many times" when discussing lidar. Additionally, one can remotely survey a site from safe locations, minimizing the danger to field crews and the traveling public. Lidar also enables a much more efficient and thorough field survey, minimizing the need for costly repeat visits to the site to collect information. The reduction in field time and the ability to acquire data from the sides of the road with static lidar or at traffic speeds with mobile lidar provide significant safety benefits over typical surveying. The comprehensive information provided by lidar greatly improves the detail in models used throughout the design process. The additional information that is resolvable in lidar data enables topography and other features to be modeled at a higher level of detail and accuracy over traditional techniques. The detailed, 3D virtual world encapsulated in a lidar point cloud provides personnel in the transportation agency with an enhanced understanding of the field conditions and variability throughout the site and, hence, reduces uncertainty in decision-making.

Figure 1.1. Mobile lidar system (Leica Pegasus:Two) owned and operated by Oregon DOT.

An important feature of the mobile lidar system is georeferencing, i.e., the assignment of precise, 3D spatial coordinates in a defined coordinate system to each point in a lidar point cloud. Georeferencing can be completed directly with the combination of components included on the scanner (e.g., GNSS-aided inertial measurement systems); however, for highest accuracy applications, rigorous survey control points are often established. Color and intensity values are often provided with lidar data sets as additional attributes to accompany the X,Y, Z spatial coordinates of points (figures 1.2 and 1.3). In particular, intensity values are a measure of backscattered signal strength and contain information on surface characteristics, including reflectance (Olsen et al. 2018).

Figure 1.2 MLS point cloud mapped with RGB color values

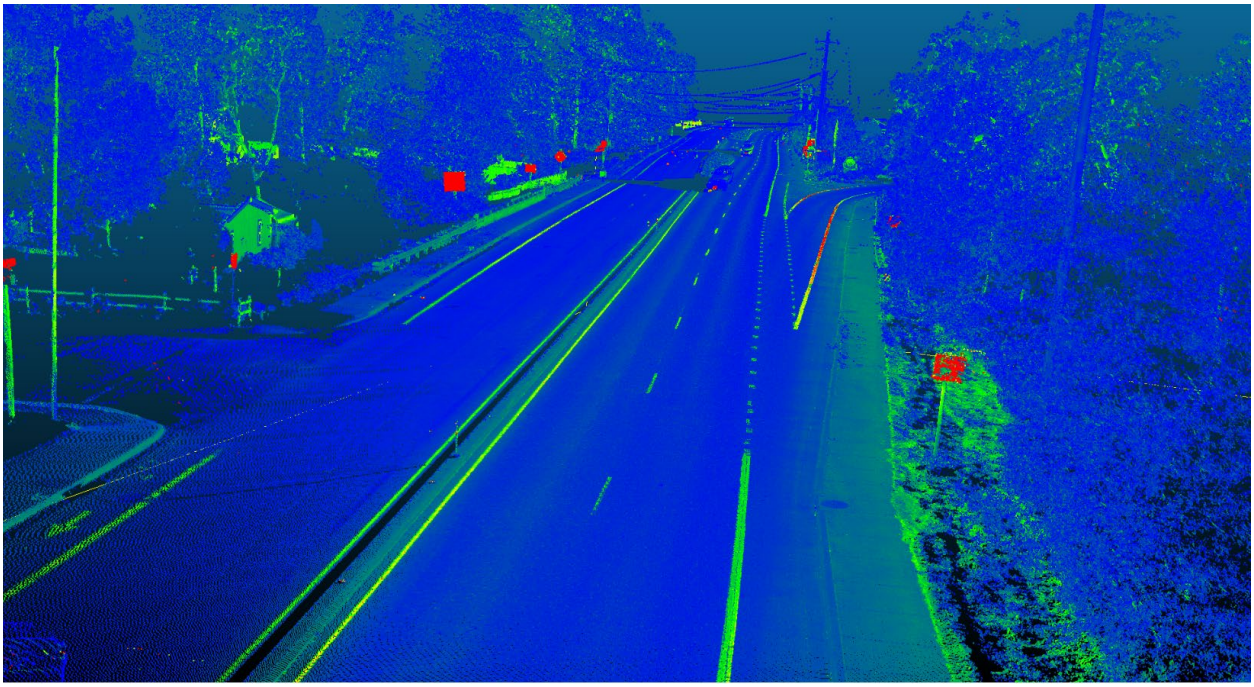

Figure 1.3 MLS intensity values. Red, green, and blue points indicate high, intermediate, and low levels of intensity.

The raw intensity values are generally provided as uncalibrated digital numbers, and in addition to surface reflectance at the laser wavelength, they are also a function of several extraneous variables related to the environment, system, and acquisition parameters (Kashani et al. 2015). Examples of these extraneous variables include laser range, incidence angle, receiver aperture, system transmittance, atmospheric transmittance, beam divergence, and transmitted laser power. A significant number of lidar intensity correction and radiometric calibration procedures have been developed with the goal of removing the effects of these environmental and system variables to provide values that better represent surface reflectance. Recent research has investigated the potential use of mobile lidar for retroreflectivity evaluation. For example, Che et al. (2019) developed and tested operational procedures to generate retroreflectivity data from ODOT's mobile scanner. Figure 1.4 shows an example validation test of the estimated retroreflectivity values extracted from mobile scanner data using two profilers operating on the left lane and right lane, in which the lidar-derived retroreflectivity estimates provide a high degree of consistency with the ground truth retroflectivity.

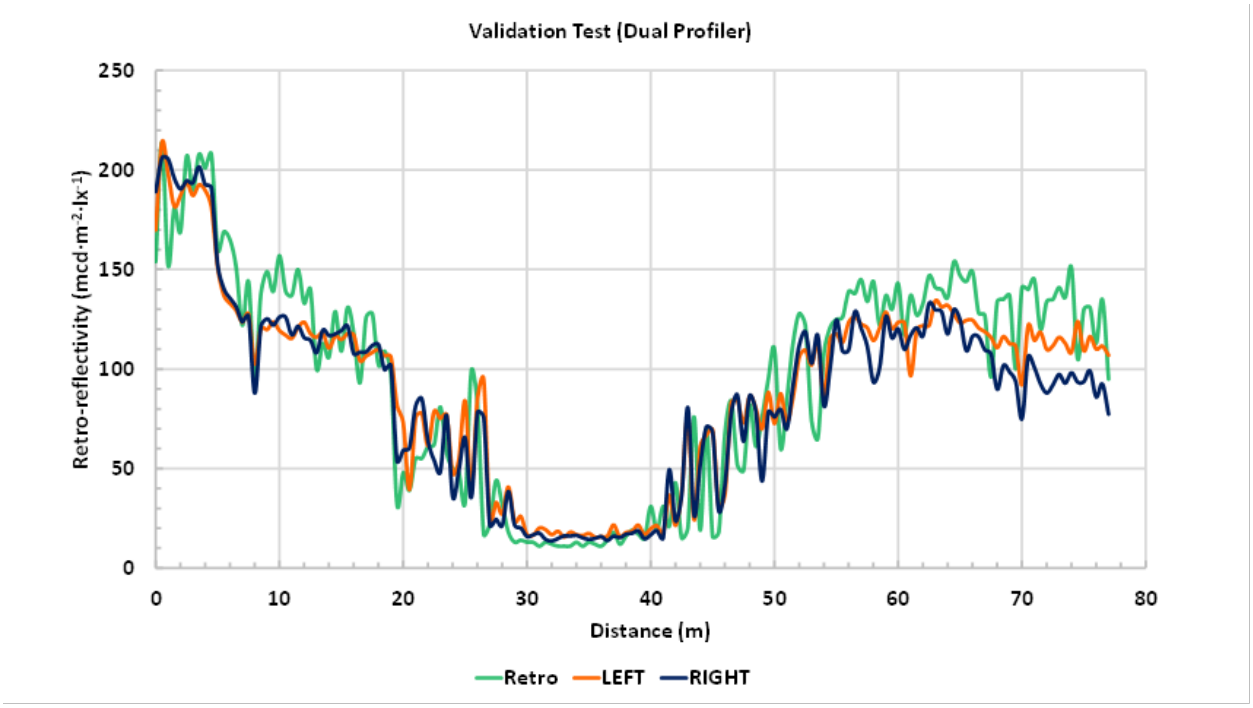

Figure 1.4. Validation test of the estimated retroreflectivity with ground truth (Che et al., 2019)

While the results of this previous work have demonstrated great promise, automated road marking extraction from MLS data has remained an open challenge because of variable noise and road conditions. Several approaches have been developed but have generally been designed for new markings with minimal wear, rather than existing markings, and only tested over relatively short sections of roadway with minimal variance in highway geometry (Kumar et al. 2014; Yu et al. 2014; Zhang et al. 2016; Soilán et al. 2017; Yang et al. 2018). To address this problem, the research team developed an efficient and robust lane marking extraction tool (Jung et al. 2019), which is now being actively used by ODOT to evaluate road marking conditions on the Oregon highway network. However, there are some limitations in using the tool because it was designed to extract only linear or smoothly curved lane markings. Also, transportation personnel have expressed increasing demands for classification of different types of road

markings. This research addressed these challenges by presenting a novel approach for efficient, reliable extraction and classification of complex road markings.

The remainder of this report is organized as follows: Chapter 2 outlines the developed road marking extraction and classification methods in detail. Chapter 3 discusses a comparison of the use of single profiler versus dual profiler data and an evaluation of the robustness of the developed approach when used with a variety of MLS data sets. Chapter 4 introduces a development version of the graphical user interface for the road marking extraction tool. Chapter 5 highlights the strengths and limitations of the developed approach and provides potential directions for future work.

CHAPTER 2. METHODS

2.1. Overview

The proposed approach can be divided into three principal steps: road surface extraction, road marking extraction, and road marking classification.

For road surface extraction, ground filtering followed by slope filtering are applied by using the rich geometric information of a point cloud to extract the road surface, including road markings. Subsequently, the extracted road surface point cloud data are rasterized into 2D to generate an image using the radiometric intensity information.

Otsu's segmentation is performed on this image to segment high-intensity pixels, which are likely to represent road markings. However, the segmentation may include some incorrect markings (false positives) because the intensity values are sensitive to changes in the range and incidence angles. To reduce those false positives while preserving actual road markings, the road surface image is partitioned into a set of blocks along the road direction, and Otsu's segmentation is applied for each partitioned block. Subsequently, a high-pass filtering and iterative morphological bridge operation is proposed to refine the segmented road markings.

Lastly, for road marking classification, common linear lane markings with lengths greater than a predefined threshold length are first segmented, and then remaining markings are classified by using a template matching model. To generate training data for the matching process, we collected a set of templates from MLS data and also created additional synthetically modified data by using a data augmentation approach to account for a variety of marking conditions, such as different orientation, skewness, and scale. The consecutive steps of the proposed approach are shown in figure 2.1.

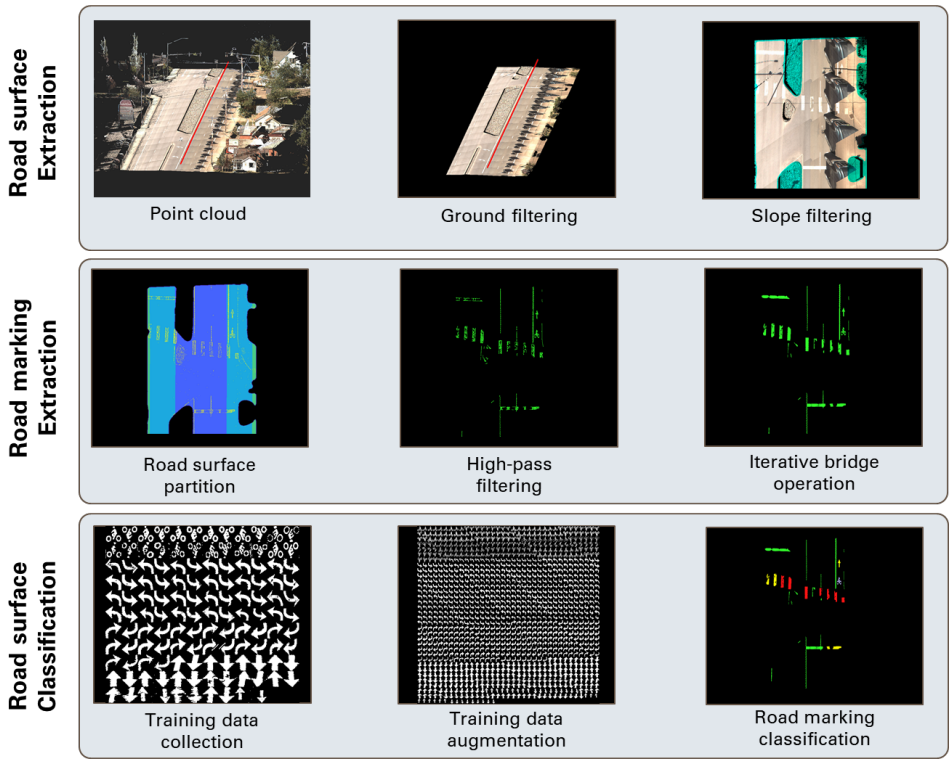

Figure 2.1. Key steps in the proposed road marking extraction and classification approach

2.2. Road Surface Extraction

Typically, the acquired MLS data include many points that are returned from various objects present within the scene (figure 2.1), making it difficult to separate road markings from other objects. To improve the detection rate of road markings as well as processing speed, it is desirable to first segment the ground surface points that are likely to include road markings. To that end, the 3D mobile lidar data are rasterized into a horizontal plane to generate a binary image that represents the occupied pixels containing at least one point within the cell area as 1 and the others as 0. The trajectory data (i.e., path of the vehicle or, more specifically, mobile lidar unit) are also rasterized onto the same binary image. Subsequently, a morphological dilation operation is performed for the rasterized trajectory to identify the area within a user-defined distance from the trajectory. The points within the area are subsequently identified on the basis

of their projected location onto the image. Figure 2.3(a) shows a point cloud extracted by the proposed horizontal filtering.

The extracted mobile lidar data may still include some non-ground points over the road surface that need to be further removed. To that end, the filtered points are clustered by using a Euclidean clustering algorithm (Ubbink, 2019), which ensures that the minimum distance between the clusters is greater than the predefined distance (Δ). Subsequently, the segment with the largest number of points is extracted as a ground surface, as shown in figure 2.3(b). The Euclidean clustering may be time-consuming as the number of points increases. To speed up the process, we implemented a voxel-based subsampling process proposed by Jung et al. (2020), which organizes the point cloud into a regularized 3D grid cell and returns the centroid and indices for each point, allowing the number of point inputs to be greatly reduced. This is particularly useful for reducing the computational burden for the Euclidean distance clustering by balancing the point density between the sparse (far from the trajectory) and dense (near the trajectory) areas.

Figure 2.2 Original point cloud.

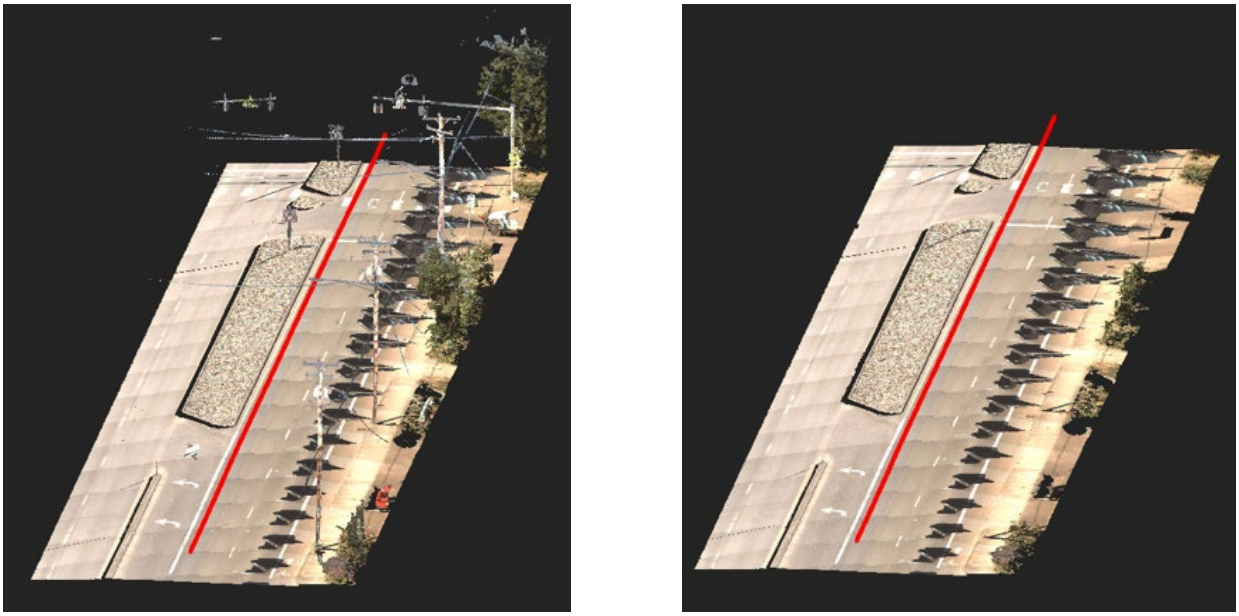

(a) (b)

Figure 2.3. Ground filtering: (a) horizontal and (b) vertical filtering. The red line indicates the MLS vehicle trajectory

The point cloud extracted by the horizontal and vertical filtering may still include some non-road objects, such as a sidewalk, a median, or some grass areas near the road surface. To remove the non-road objects, the ground points are rasterized into a 2D elevation image by using the z-values. Because the road surface tends to be relatively flat and smooth, a slope image is calculated from the elevation image by using a Sobel operator (Pan et al. 2019) to filter out the pixels with high slope values. The proposed slope filtering requires a predefined threshold value, which can vary depending on the condition of the road surface. Therefore, a dynamic thresholding strategy is proposed to account for the different road conditions.

First, the trajectory is rasterized onto the slope image. A morphological dilation operation is applied to extract the area within one meter from the trajectory. Then, the average (μ) and standard deviation (s) of the slope values within the area are calculated. Finally, the condition to remove the pixels (p) with high slope values is defined as

$$p_{i=1:n}^{slope} > \mu + \tau * s \tag{2.1}$$

where n is the number of occupied pixels, and τ is the scale factor. Figure 2.4 illustrates an example of road surface extraction using the proposed slope filtering in which one can see that medians and grass areas in the sidewalk have been successfully removed.

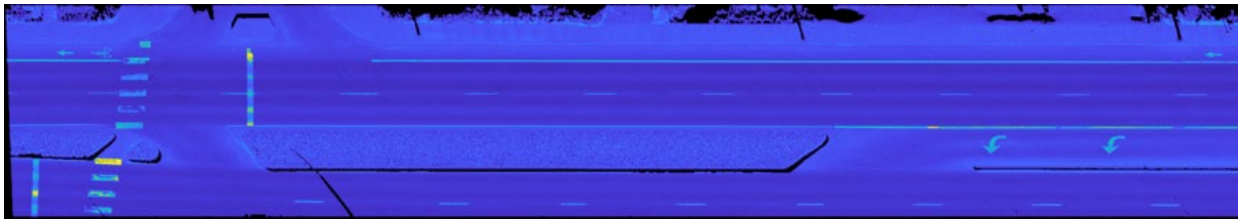

(a)

(b)

Figure 2.4 Road surface extraction: (a) before and (b) after slope filtering

2.3. Road Marking Extraction

In this step, the extracted road surface is segmented into the road markings and other objects by using the intensity values. Because the intensity values are sensitive to changes in the range and incidence angles, applying a single threshold would lead to over- or under-segmentation (Che et al. 2019). In the literature, a commonly used approach, which was also adopted in this study, is to partition the roadway into a set of blocks along the road direction and segment the road marking separately (Yang et al. 2018). The trajectory rasterized in the previous road surface extraction is used again to provide dilated binary images with a 5-m, disk-shaped structuring element to partition the road surface into smaller longitudinal blocks, as illustrated in figure 2.5. On each partitioned block, the road marking segmentation is performed separately by using Otsu's segmentation, which calculates the histogram and finds the value that maximizes the variance between the clusters (Otsu et al. 1979). To increase the contrast of the markings against the surrounding pavement, a contrast-limited adaptive histogram equalization algorithm

is also applied. As a result, each intensity block is binarized into two groups: the high-intensity group that is likely to represent the road markings and the low-intensity group that represents other, non-road marking objects.

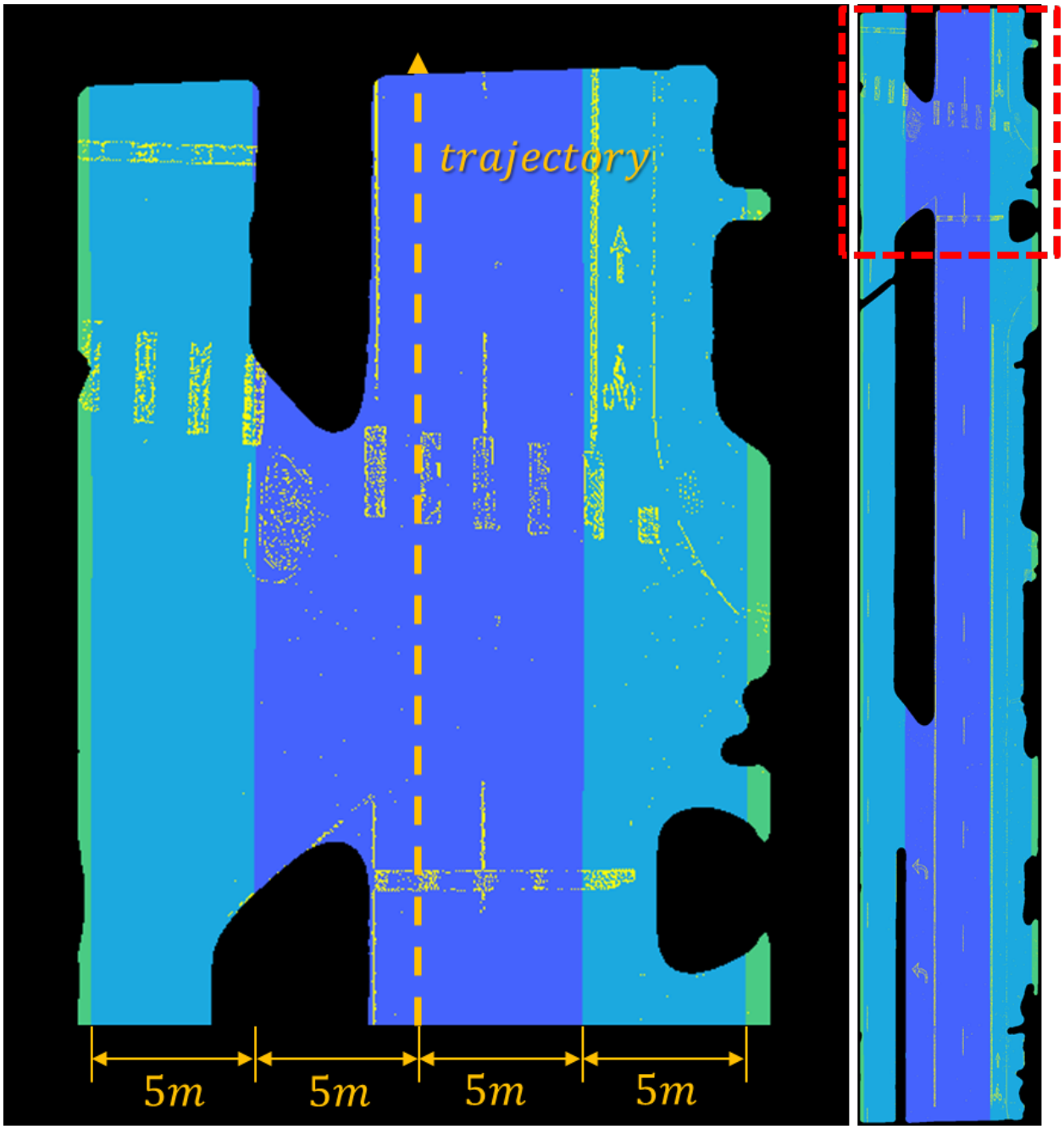

Figure 2.5 Road marking extraction on partitioned road surface blocks

Road marking segmentation is a challenging task because of several factors that generate noise. For example, the MLS points returned from grass and soil surfaces tend to produce high-intensity values because of the improved incidence angle, making it difficult to separate them from road markings (Kumar et al. 2014). As a result, the segmented road markings may include some false positives that also have high-intensity values. To address that, use of high-pass filtering (Cheng et al. 2016) is proposed, which greatly reduces false positives by highlighting only the pixels with abrupt changes in intensity values. Figure 2.6 shows the remaining pixels after high-pass filtering has been applied. Subsequently, a morphological closing operation (i.e., dilation followed by erosion) is performed to aggregate the fragmented potential road markings (figure 2.6a). The high-pass filtering tends to break down the correct road markings into smaller segments because of a halo effect. To address this problem, the fragmented road markings are reconstructed by iteratively applying a morphological bridge operation, which connects two neighbor objects on the binary image. Figure 2.6b depicts the road markings before and after the iterative bridge morphological operation has been applied.

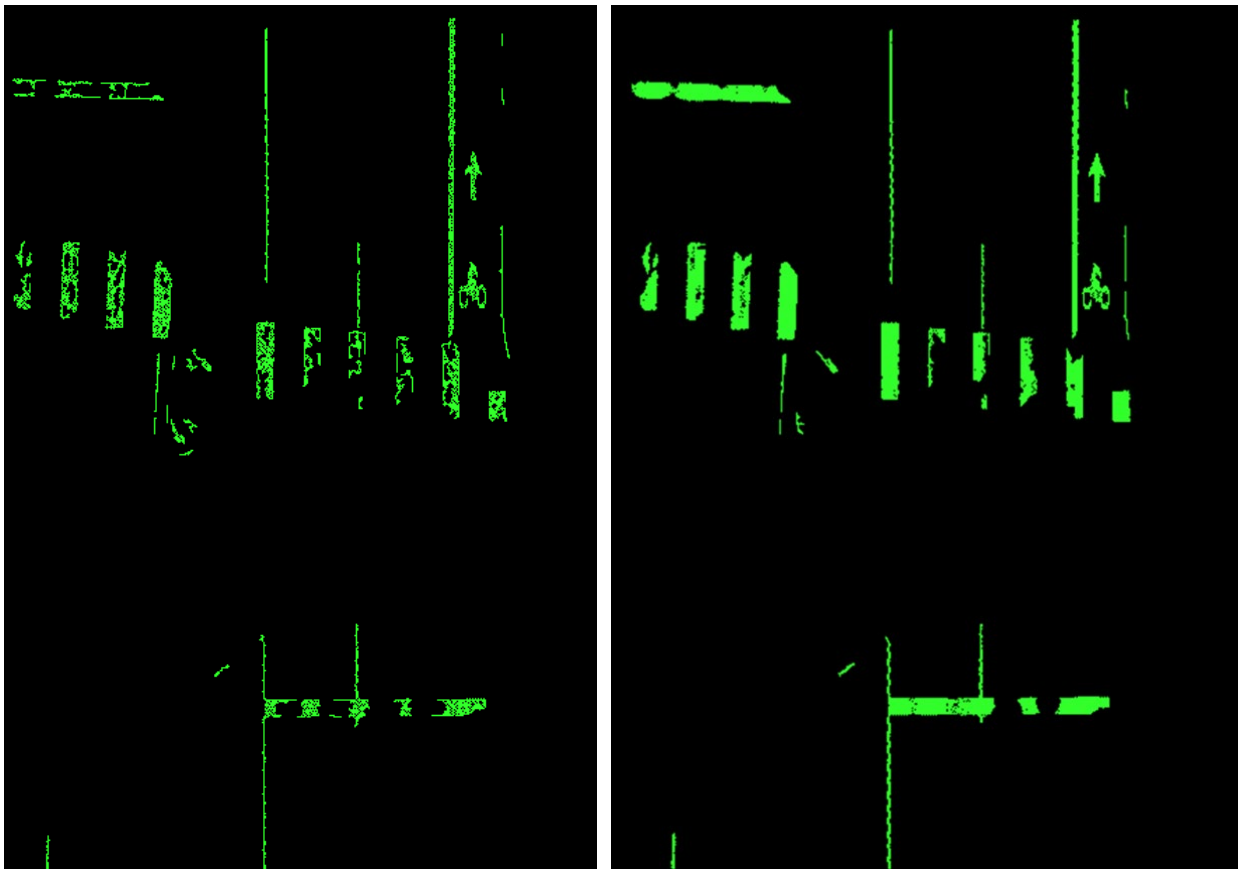

(a) (b)

Figure 2.6. Refinement of road markings using the morphological bridge operation: (a) before and (b) after refinement.

2.4. Road Marking Classification

In this step, the extracted road markings are classified by using a template matching method, which calculates the matching score between templates and the input image. We have collected a set of templates from the MLS data and markings images available online. Before template matching, the extracted markings are isolated by using a connected component analysis (Jung et al. 2014) and are evaluated to separate the lane markings by using two conditions. First, for each marking, an ellipse is fitted by computing the second-order moments, and the markings with a major axis greater than a predefined value (4 m was used in this study) are identified as

lane markings. Second, the markings with a width smaller than a predefined value (0.2 m was used in this study) are identified as lane markings. A morphological erosion operation is performed with a disk-shaped structuring element of 0.1 m, enabling the extraction of most of the lane markings from others.

Once the lane markings have been separated, each remaining marking is resized by using a bilinear interpolation method to match the size with template images. Because the collection of template images is labor intensive and time consuming, a data augmentation technique is adopted (figure 2.7) in which the collected marking images are rotated and skewed by using an affine transformation to generate augmented template data. Next, the extracted and resized markings are input into a template matching model (Kroon, 2020) that calculates the normalized cross-correlation on the basis of image texture. Figure 2.8 shows an example of the road markings classified by using the template matching method. Overall, the results demonstrated that the proposed approach effectively extracts and classifies six common types of road markings (i.e., pedestrian crosswalk, bike lane, car lane, and left arrow, straight arrow, and right arrow markings). In the example, however, note that some parts of crosswalk markings were misclassified as lane marking because they were worn-out or as straight arrows because of insufficient training data, indicating the need for future work to refine those results.

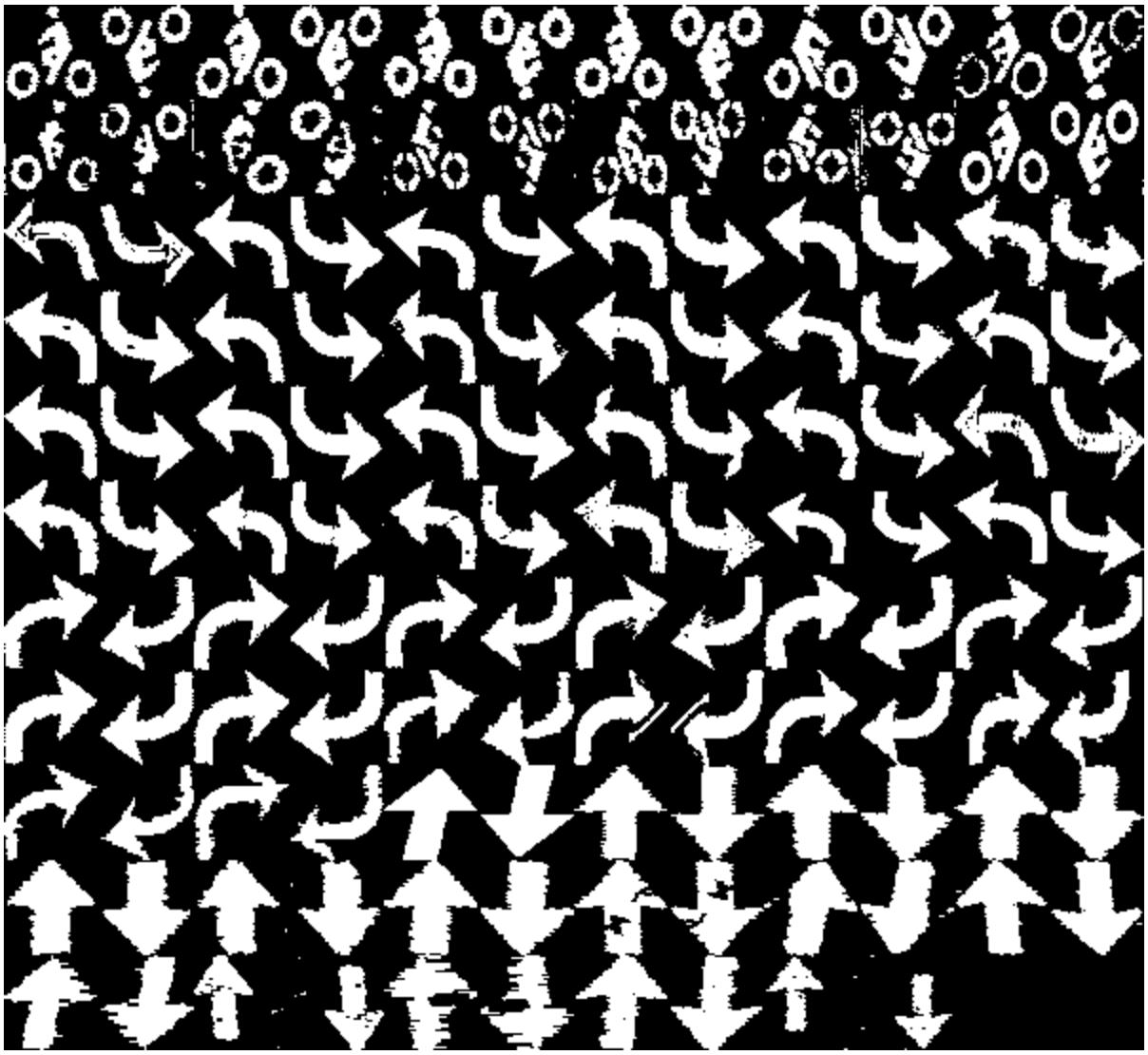

Figure 2.7. Template data collected from the MLS data and markings images available online

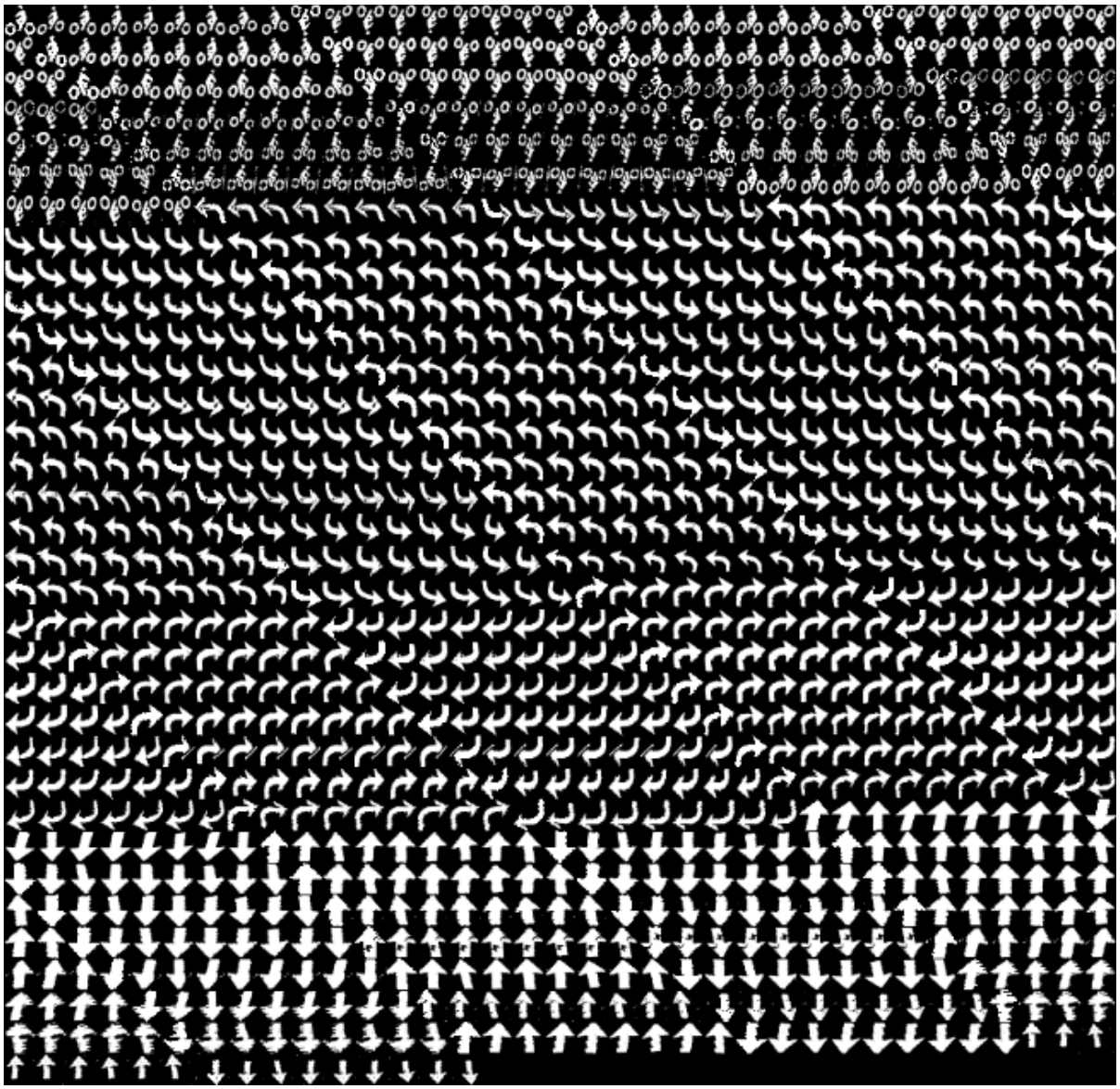

Figure 2.8. Augmented template data using an affine transformation

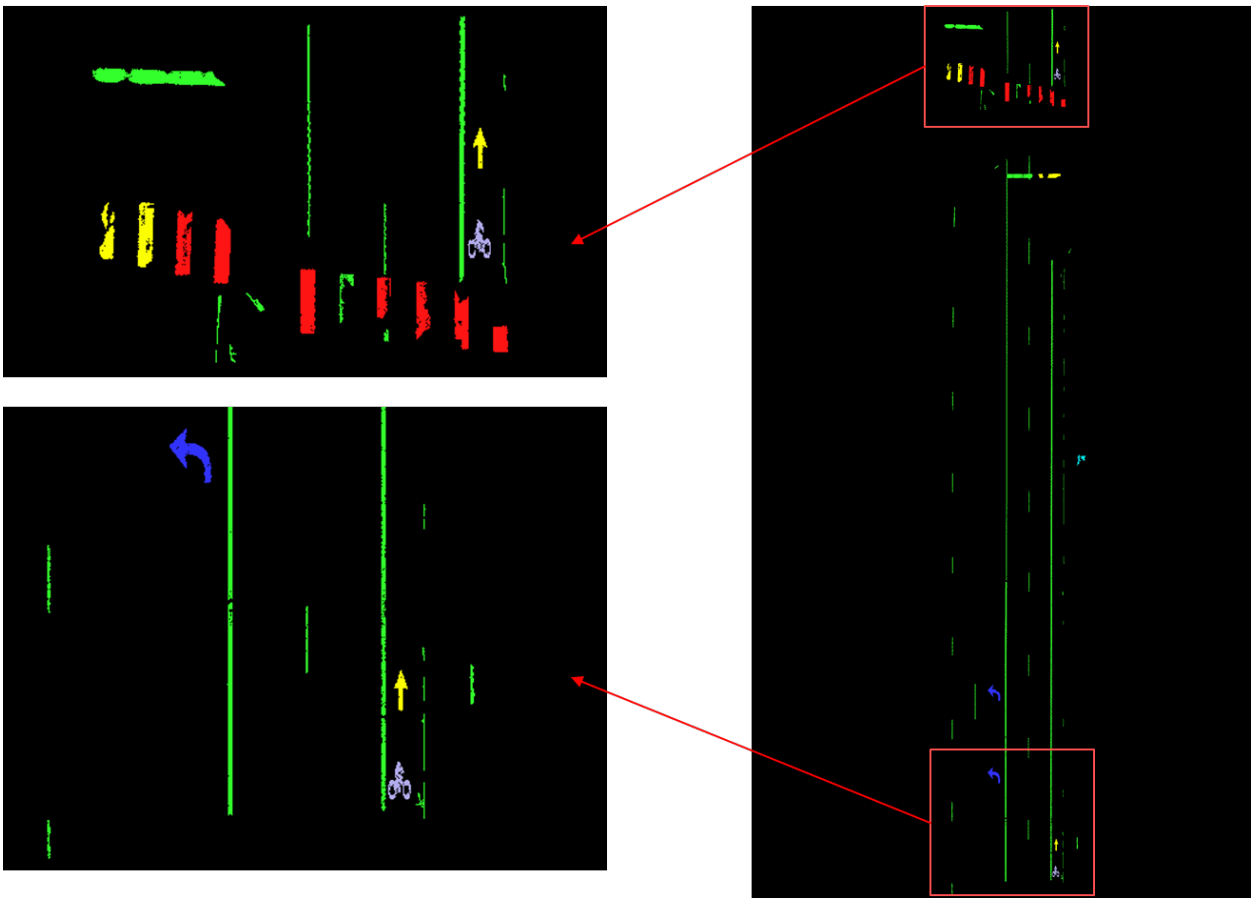

Figure 2.9 Classification of complex road markings in which each color represents a different type of road marking.

CHAPTER 3. RESULTS

3.1. Evaluation of Single Profiler versus Dual Profiler Data

Some recent MLS systems support a dual profiler configuration with two laser profilers to improve coverage across the scene. For example, ODOT's MLS scanner operates in a dual profiler configuration with scanners pointed at -30° and +60° to the direction of travel. This means that one laser looks forward while the other looks in reverse. The dual profiler increases the point density and provides data from a greater variety of acquisition geometries. This work found that the dual profiler is particularly advantageous in capturing road markings distant from the lane in which the MLS system operates.

However, a challenge with the dual profiler is that the same object captured in different profilers can represent intensity variations. Therefore, data from each profiler should be processed individually and merged later. The dynamic thresholding method presented in Chapter 2 is particularly useful for processing multiple profiler data. Figure 3.1 evaluates the markings extracted from single profiler and dual profiler data, respectively. Both results show similar trends overall, but one can clearly see that the dual profiler results are more robust in preventing false negatives than the single profiler.

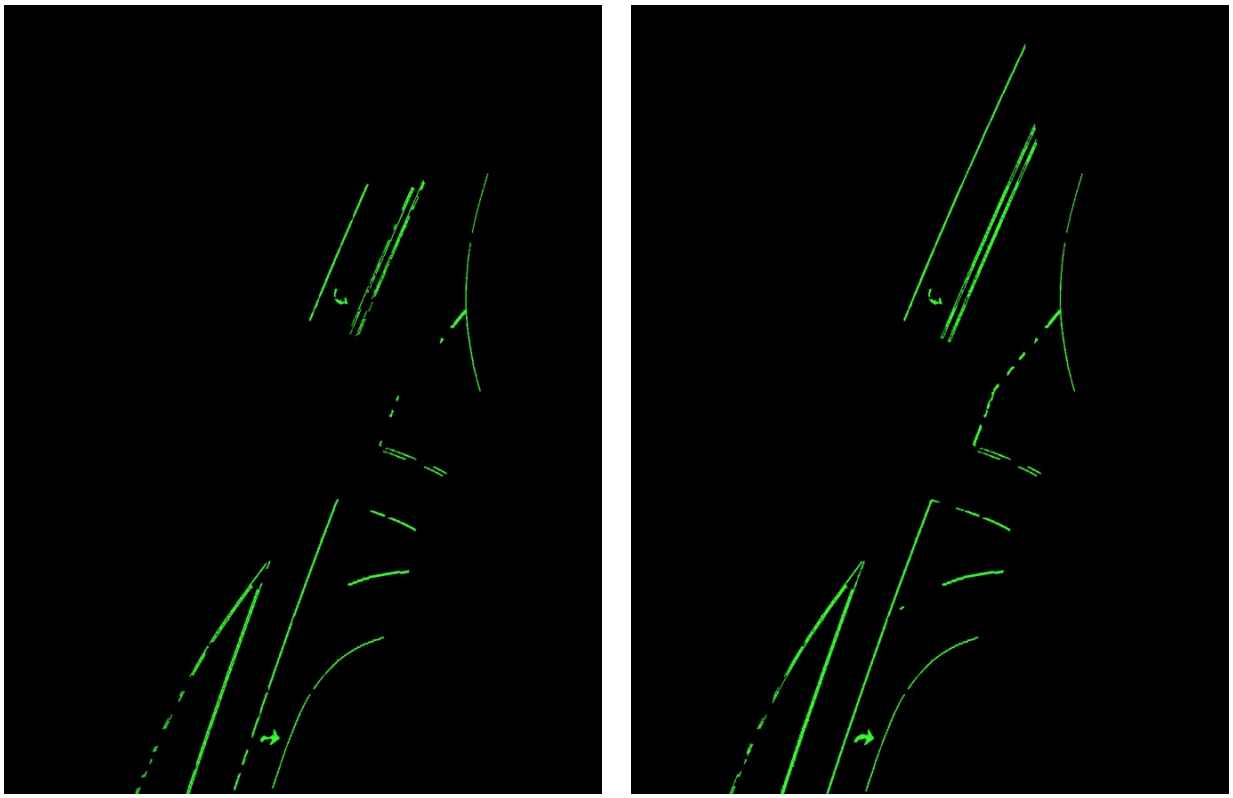

(a) (b)

Figure 3.1 Road markings extracted from (a) single and (b) dual profiler data

3.2. Evaluation of RoME v1.3 versus RoME v2.0

This section provides comparative results of RoME v1.3, our previous version of the road marking extraction tool, and RoME v2.0, the updated version developed through this PacTrans project. Several test data sets were used (table 3.1). Figures 3.2 through 3.6 include three images: (a) a rasterized point cloud with intensity values, (b) road markings extracted with RoME v1.3, and (c) those extracted with RoME v2.0. Note that RoME v1.3 divided the point cloud data into smaller sections (e.g., 10-m intervals) to extract smoothly curved lane markings, resulting in the extracted and combined lane markings being linearized in figures 3.2 through 3.6 (b). Additionally, RoME v1.3 was not capable of extracting highly curved or complex markings and was also sensitive to some false positives (highlighted with red circles in figures 3.2 through

3.6 (b)) near the roadways. Figures 3.2 through 3.6 (c) demonstrate that these problems were successfully overcome by the enhanced program developed in this project, RoME v2.0. Further, RoME v2.0 can classify the extracted markings, which are denoted by different colors in figures 3.3, 3.5, and 3.6. It is also important to note that RoME v2.0 is significantly faster than RoME v1.3, as shown in table 3.1.

Table 3.1 Test data sets acquired by Oregon DOT's MLS system (Leica Pegasus 2)

No.	Location	Profiler configuration	Number of points (millions)	Length (meters)	Process time (seconds)	
					RoME v1.3	RoME v2.0
1	Spangler	Dual	16.9	301.3	105.3	70.6
2	Spangler	Dual	15.8	546.7	199.3	153.0
3	I-5 highway	Single	19.1	1012.5	318.8	171.1
4	Philomath	Single	19.3	449.6	168.7	111.3
5	Philomath	Single	19.4	352.5	175.0	93.8

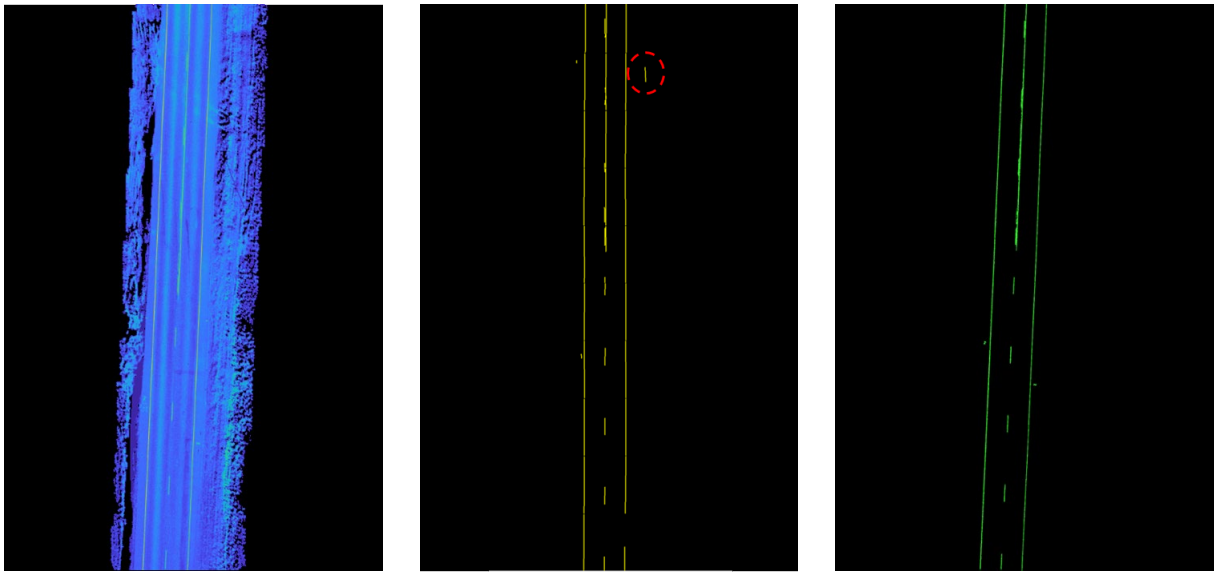

(a) (b) (c)

Figure 3.2 Example road markings extracted from data set 1: (a) intensity image; (b) RoME v1.3; and (c) RoME v2.0 results

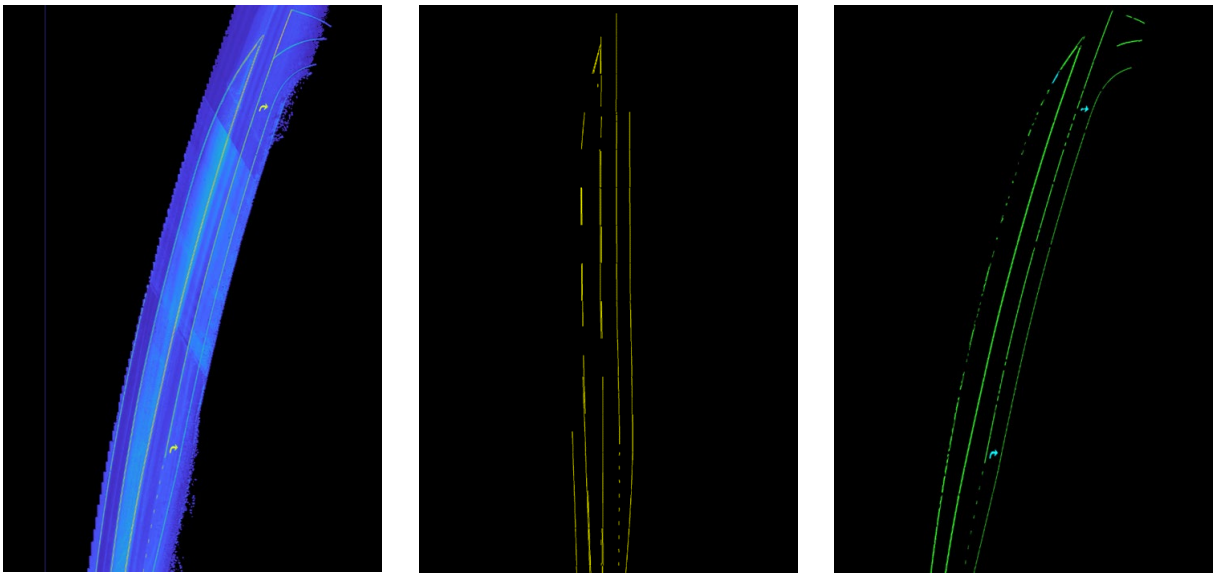

(a) (b) (c)

Figure 3.3 Example road markings extracted from data set 2: (a) intensity image; (b) RoME v1.3; and (c) RoME v2.0 results

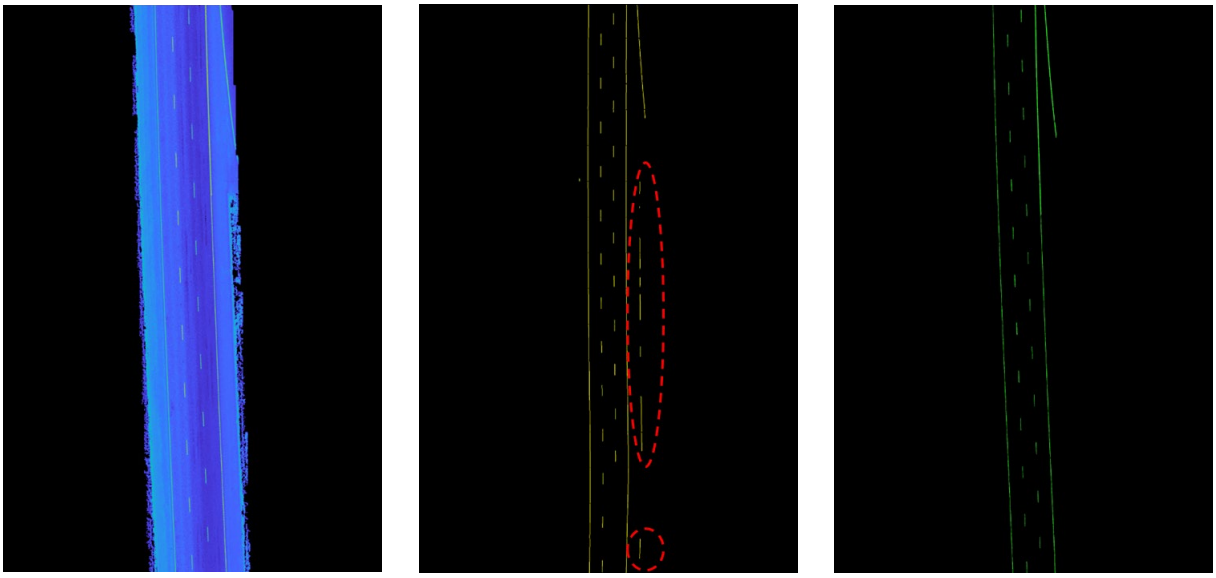

(a) (b) (c)

Figure 3.4 Example road markings extracted from data set 3: (a) intensity image; (b) RoME v1.3; and (c) RoME v2.0 results

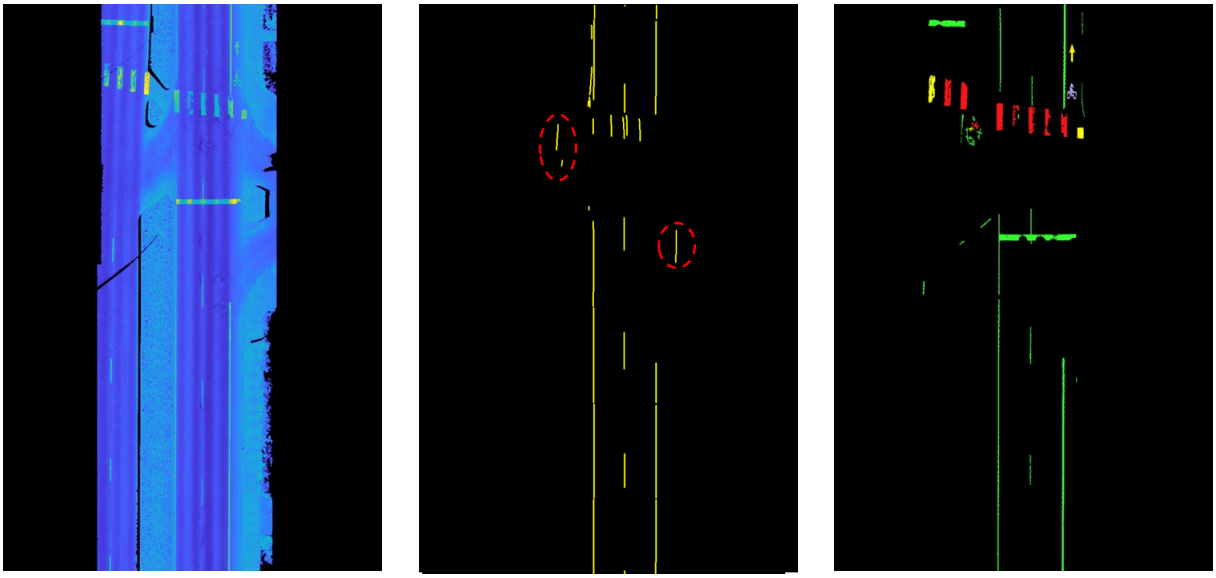

(a) (b) (c)

Figure 3.5 Example road markings extracted from data set 4: (a) intensity image; (b) RoME v1.3; and (c) RoME v2.0 results

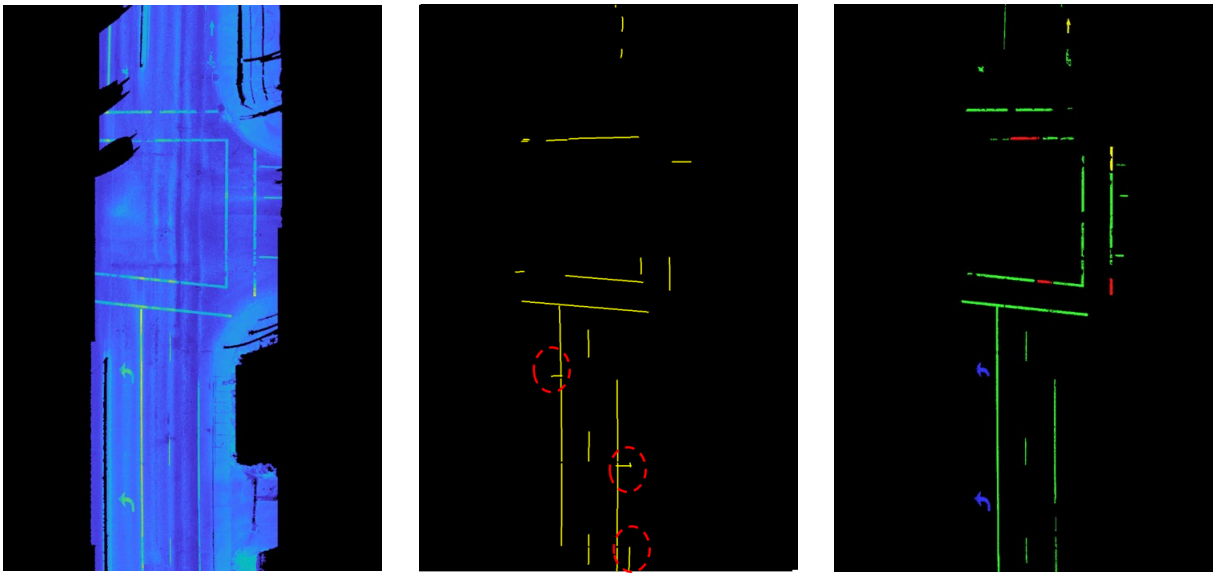

(a) (b) (c)

Figure 3.6 Example road markings extracted from data set 5: (a) intensity image; (b) RoME v1.3; and (c) RoME v2.0 results

CHAPTER 4. ROAD MARKING EXTRACTION TOOL

Figure 4.1 shows a beta version of the new road marking extraction tool (ver. 2.0). This tool is designed for maintenance personnel, engineers, and other authorities in transportation departments who need this information to help make appropriate decisions in evaluating road markings. The RoME v2.0 contains a simple interface that does not require users to have extensive knowledge of the program or point cloud data in order to run it successfully. The inputs to the program are the point cloud(s) in ASPRS LAS v1.2 format, which is the current version provided by ODOT, and trajectory (asciitrj) data obtained by a mobile lidar unit. The outputs include a road marking point cloud that can be utilized in many decision making processes and applications, such as retroreflectivity evaluations. At this time, road marking extraction has been tested and evaluated with ODOT's current mobile lidar system (Leica Pegasus:Two) and may not produce correct results for other systems. The system is currently capable of classifying only pedestrian crosswalk, bike lane, car lane, left arrow, straight arrow, and right arrow markings. Users need to retrain the template-matching model to classify other types of road markings. Also, some features that were available in RoME 1.3, such as saving CSV files and retro-reflectivity evaluation, are currently not available. These will be integrated into a future release.

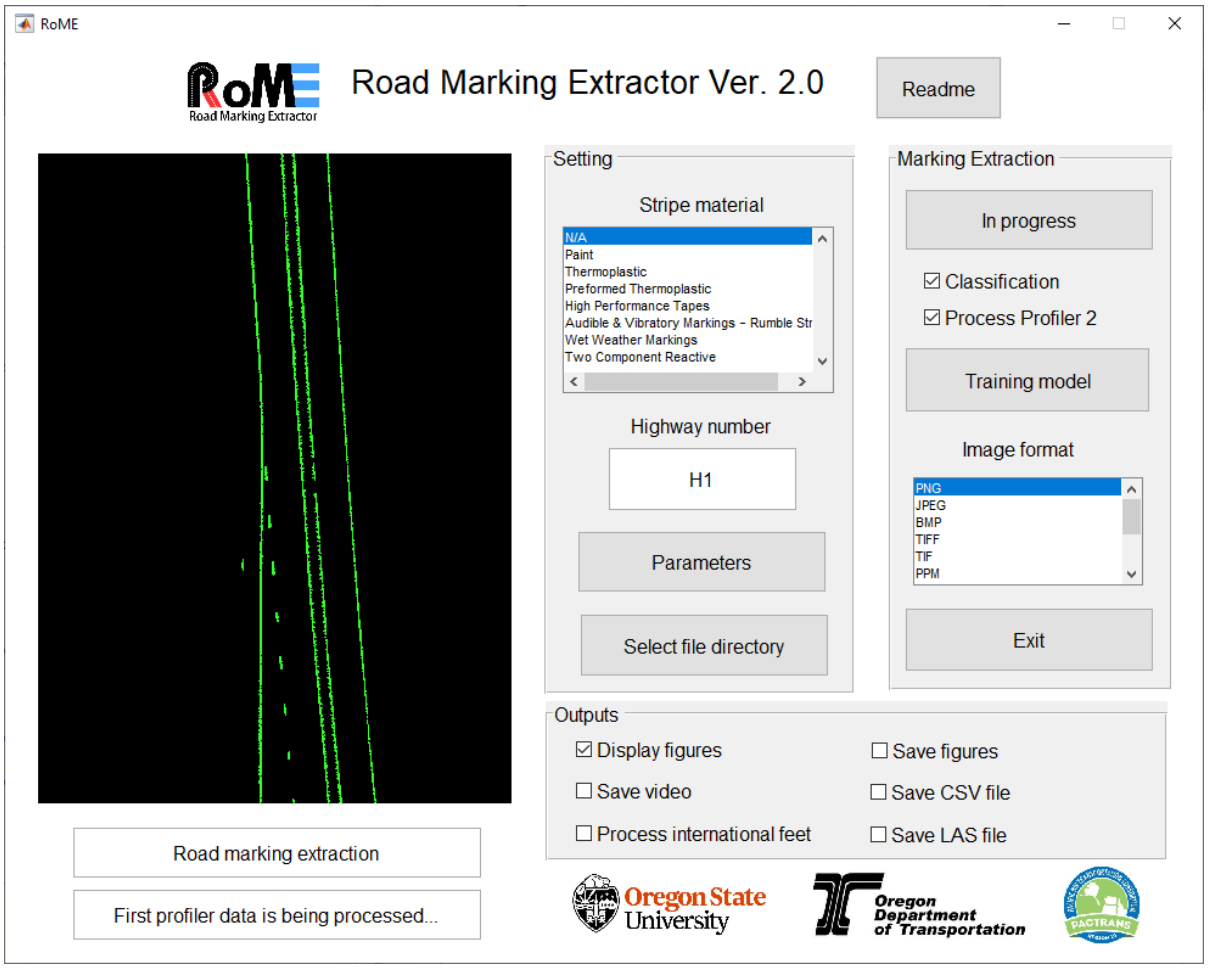

Figure 4.1 Road Marking Extraction (RoME) tool v2.0

CHAPTER 5. CONCLUSIONS

Pavement markings are an important traffic control device, enhancing both the safety and efficiency of various modes of transportation by aiding vehicles, bicyclists, and pedestrians in effectively navigating the transportation network. In this research, we developed advanced techniques to extract and classify complex markings (e.g., pedestrian crosswalk, bike lane, car lane, left arrow, straight arrow, and right arrow markings). Broadly, the proposed approach can be divided into three principal steps: road surface extraction, road marking extraction, and road marking classification.

In the road surface extraction step, by using the geometric information of the point cloud and trajectory data, the road surface points that are likely to include road markings are segmented. Next, in the road marking extraction step, the road surface intensity values are rasterized into a 2D image in which Otsu's method is used to segment high-intensity pixels as candidate road markings. Furthermore, to detect road markings in noise, dynamic thresholding segmentation and high-pass filtering approaches are applied. Finally, for road marking classification, a template matching is performed with augmented, pre-classified training data sets. Experimental results with a variety of MLS data sets demonstrated that the developed program successfully extracts highly curved and complex road markings, with significantly fewer false positives and false negatives than the previous version of the road marking extraction tool (RoME v1.3). The developed program includes a user-friendly graphic user interface that can be operated without extensive knowledge of the algorithms behind the scenes within the program. This program will support informed decision making by DOT management for improved maintenance of pavement markings, which will also lead to improved mobility with technologies such as autonomous vehicles.

There are some key recommendations to use the developed program effectively. The program has been tested and evaluated with ODOT's MLS system (Leica Pegasus:Two) and will require some adjustment of settings to use data acquired with other systems. If dual profiler data are available, it is generally recommended to use them to reduce false negatives. The developed approach is currently capable of classifying pedestrian crosswalk, bike lane, car lane, left arrow, straight arrow, and right arrow markings. To classify other types of road markings, users will need to collect new data sets to retrain the template model. Also, other machine learning techniques, such as a convolutional neural network, could be integrated into the classification process; however, these techniques would require a much larger amount of training data to achieve good performance.

REFERENCES

ASPRS, 2008, LAS specification version 1.2. <https://www.asprs.org/a/society/committees/standards/asprs_las_format_v12.pdf>. Accessed June 11, 2020.

Che, E., Olsen, M.J., Parrish, C.E. and Jung, J., 2019. *Pavement Marking Retroreflectivity Estimation and Evaluation using Mobile Lidar Data*. Photogrammetric Engineering & Remote Sensing, 85(8), pp.573-583.

Cheng, M., Zhang, H., Wang, C. and Li, J., 2016. *Extraction and classification of road markings using mobile laser scanning point clouds*. IEEE Journal of Selected Topics in Applied Earth Observations and Remote Sensing, 10(3), pp.1182-1196.

Jung, J., Hong, S., Jeong, S., Kim, S., Cho, H., Hong, S. and Heo, J., 2014. *Productive modeling for development of as-built BIM of existing indoor structures*. Automation in Construction, 42, pp.68-77.

Jung, J., Che, E., Olsen, M.J. and Parrish, C., 2019. *Efficient and robust lane marking extraction from mobile lidar point clouds*. ISPRS journal of photogrammetry and remote sensing, 147, pp.1-18.

Jung, J., Che, E., Olsen, M.J. and Shafer, K.C., 2020. *Automated and efficient powerline extraction from laser scanning data using a voxel-based subsampling with hierarchical approach*. ISPRS Journal of Photogrammetry and Remote Sensing, 163, pp.343-361.

Kashani, A.G., Olsen, M.J., Parrish, C.E. and Wilson, N., 2015. *A review of LiDAR radiometric processing: From ad hoc intensity correction to rigorous radiometric calibration*. Sensors, 15(11), pp.28099-28128.

Kroon., D. 2020. *Fast/Robust Template Matching*. MATLAB Central File Exchange. <https://www.mathworks.com/matlabcentral/fileexchange/24925-fast-robust-template-matching>. Accessed May 20, 2020.

Kumar, P., McElhinney, C.P., Lewis, P. and McCarthy, T., 2014. *Automated road markings extraction from mobile laser scanning data*. International Journal of Applied Earth Observation and Geoinformation, 32, pp.125-137.

Olsen, M.J., Roe, G.V., Glennie, C., Persi, F., Reedy, M., Hurwitz, D., Williams, K., Tuss, H., Squellati, A., and Knodler, M., 2013a. *Guidelines for the use of mobile lidar in transportation applications*. TRB NCHRP Final Report 748, p194.

Olsen, M.J., Roe, G.V., & Raugust, J., 2013b. U*se of advanced geospatial data tools, technologies, and Information in DOT projects*, NCHRP Synthesis 446, Topic 43-09, p.87

Olsen, M.J., Parrish, C.E., Che, E., Jung, J. and Greenwood, J., 2018. *LIDAR for Maintenance of Pavement Reflective Markings and Retroreflective Signs Vol. I: Retroflective Pavement Markings* (No. FHWA-OR-RD-19-03).

Otsu, N., 1979. *A threshold selection method from gray-level histograms*. IEEE transactions on systems, man, and cybernetics, 9(1), pp.62-66.

Pan, Y., Yang, B., Li, S., Yang, H., Dong, Z. and Yang, X., 2019. *Automatic road markings extraction, classification and vectorization from mobile laser scanning data*. The International Archives of the Photogrammetry, Remote Sensing & Spatial Information Sciences, Volume XLII-2/W13, pp.1089-1096.

Soilán, M., Riveiro, B., Martínez-Sánchez, J. and Arias, P., 2017. *Segmentation and classification of road markings using MLS data*. ISPRS Journal of Photogrammetry and Remote Sensing, 123, pp.94-103.

Ubbink, J.T., 2019. *The development of a digital design workflow for the surgical obturator*. Master's thesis, University of Twente.

Yang, M., Wan, Y., Liu, X., Xu, J., Wei, Z., Chen, M. and Sheng, P., 2018. *Laser data based automatic recognition and maintenance of road markings from MLS system*. Optics & Laser Technology, 107, pp.192-203.

Yu, Y., Li, J., Guan, H., Jia, F. and Wang, C., 2014. *Learning hierarchical features for automated extraction of road markings from 3-D mobile LiDAR point clouds*. IEEE Journal of Selected Topics in Applied Earth Observations and Remote Sensing, 8(2), pp.709-726.

Zhang, H., Li, J., Cheng, M. and Wang, C., 2016. *Rapid inspection of pavement markings using mobile lidar point clouds*. International Archives of the Photogrammetry, Remote Sensing & Spatial Information Sciences, 41, pp.717-723.